THE JOURNAL OF BIOLOGICAL CHEMISTRY VOL. 284, NO. 31, pp. 21057–21065, July 31, 2009

Prostate-specific Klf6 Inactivation Impairs Anterior Prostate Branching Morphogenesis through Increased Activation of the Shh Pathway*[S]

Received for publication, April 1, 2009, and in revised form, May 29, 2009 Published, JBC Papers in Press, June 3, 2009, DOI 10.1074/jbc.M109.001776

Ching Ching Leow[‡1], Bu-er Wang[‡], Jed Ross[§], Sara M. Chan[¶], Jiping Zha[¶], Richard A. D. Carano[§], Gretchen Frantz[¶], Michael M. Shen[‖], Frederic J. de Sauvage[‡2], and Wei-Qiang Gao[‡3]

From the Departments of [‡]Molecular Biology, [§]Tumor Biology and Angiogenesis, and [¶]Pathology, Genentech Inc., South San Francisco, California 94080 and the [‖]Herbert Irving Comprehensive Cancer Center, Columbia University College of Physicians and Surgeons, New York, New York 10032

Krüppel-like factor 6 (Klf6) belongs to a family of zinc finger transcription factors known to play a role in development and tumor suppression. Although *Klf6* is highly mutated in prostate cancer, its function in prostate development is unknown. We have generated a prostate-specific Klf6-deficient mouse model and report here a novel role for Klf6 in the regulation of prostate branching morphogenesis. Importantly, our study reveals a novel relationship between Klf6 and the Shh pathway. Klf6-deficiency leads to elevated levels of hedgehog pathway components (Shh, Ptc, and Gli) and loss of their localized expression, which in turn causes impaired lateral branching.

Klf6 belongs to the family of Krüppel-like zinc finger transcription factors that regulate cell proliferation and differentiation (1). All members of the *Klf* gene family contain a highly conserved zinc finger DNA binding domain at their C terminus and an activation domain at its N terminus, distinct to each *Klf* gene and accounting for their wide-ranging biological capabilities (2–4). Similar to other members of the Klf family (5, 6), Klf6 is reported to act as a tumor suppressor (7–10). *Klf6* has been reported to be mutated in a large percentage of human prostate tumors (7), but its function during normal development has not been elucidated.

Prostate development, specifically epithelial branching morphogenesis, is a well studied process. Outgrowth and branching of the prostate epithelial buds into the enveloping mesenchyme occur during the first 3 weeks postnatally (11). The fully developed prostate in an adult mouse is composed of three different paired lobes, referred as the anterior, ventral, and dorsal-lateral lobes. In addition, the number of main ducts and complexity of ductal branching vary among the three lobes. A number of growth factors/pathways have been implicated in regulating prostatic epithelial proliferation and differentiation, including hedgehog (Hh),[4] bone morphogenic proteins (BMPs), fibroblastic growth factors (FGFs), and Notch and Wnt pathways (12–19). For example, work done in our laboratory and others showed that sonic hedgehog (Shh) produced in the prostatic epithelium is a negative regulator of prostatic branching morphogenesis, mediated indirectly by periepithelial mesenchymal cells (12–15). In addition, while mesenchymal FGF10 stimulates prostatic epithelial growth (16), BMP4 is a mesenchymal factor that inhibits prostatic ductal budding and branching morphogenesis (17).

All *Klf* knockouts generated thus far are embryonic lethal (20–22), including the *Klf6* knock-out mice (23). Because prostate development begins in late gestation and continues postnatally, we overcame embryonic lethality to study the role of Klf6 in prostate development and tumorigenesis by generating a prostate-specific deletion of the *Klf6* gene using a Cre-lox recombination approach. We report here a novel role for Klf6 in the regulation of Shh-mediated epithelial branching morphogenesis in the anterior prostate.

MATERIALS AND METHODS

Generation, Genotyping, and Reverse Transcription-PCR of Klf6 Prostate-specific Mutant Mice—We generated prostate-specific deletion of Klf6 exons 2 and 3 by crossing $Klf6^{f/f}$ mice (C57BL/6, 129Sv) with $Nkx3.1^{Cre/+}$ (C57BL/6, 129Sv) knock-in mice, which expressed Cre recombinase from the Nkx3.1 locus.[5] The $Nkx3.1^{Cre/+}$ knock-in mice used in the crosses were phenotypically identical to the published Nkx3.1 mutant mice (25) and, thus, exhibited normal prostate development. PIN lesions were detected in $Nkx3.1^{Cre/+}$ mice only after they have been aged beyond 1 year.[6] Data presented in this report were mostly analyzed at P5, and the latest time point presented is 1 year of age, where loss of one Nkx3.1 allele did not exert any abnormal effects on prostate development. Genotyping of Klf6 mutants was done by Southern analysis for the F_0 and F_1 gen-

* This work was supported, in part, by National Institutes of Health Grant CA115985 (to M. M. S.).

[S] The on-line version of this article (available at http://www.jbc.org) contains supplemental Figs. S1–S3.

[1] Present address: MedImmune, One MedImmune Way, Gaithersburg, MD 20878.

[2] To whom correspondence may be addressed: MS#37, 1 DNA Way, South San Francisco, CA 94080. Fax: 650-225-6412; E-mail: sauvage@gene.com.

[3] To whom correspondence may be addressed: MS#37, 1 DNA Way, South San Francisco, CA 94080. Tel.: 650-225-8101; Fax: 650-225-6412; E-mail: gao@gene.com.

[4] The abbreviations used are: Hh, hedgehog; BMP, bone morphogenic protein; FGF, fibroblastic growth factor; Shh, sonic hedgehog; Micro-CT, micro-computed tomography; SMA, smooth muscle actin; H&E, hematoxylin and eosin; TCRD, T-cell receptor delta chain.

[5] Y. P. Hu, S. M. Price, Z. Chen, W. Banach-Petrosky, C. Abate-Shen, and M. M. Shen, unpublished observations.

[6] M. Shen, unpublished data.

erations (data not shown), and subsequent generations were genotyped by PCR analysis using the forward primer, 5′-GTC TCT TGA CAC CTT GAC TAT CTC TCC-3′, and the reverse primer, 5′-CTA CAG GAT TCG TCC CTC TGC-3′, from genomic DNA obtained from tail biopsies. We prepared RNA from TRIzol (Invitrogen) extractions from various prostate lobes, brain, testes, and kidney tissues. The RNA was then used for reverse transcription-PCR to confirm Klf6 deletion through detection of a 695-bp PCR product using forward primer 5′-GAA TAC TCT TGG AGT GCT AGG and reverse primer 5′-CTG CTC CTT CAG AGG TGC. RNA loading control was performed by employing a housekeeping gene called T-cell receptor delta chain (TCRD). TCRD was employed to ensure that equal RNA was loaded into each lane and was detected using forward primer 5′-CAA ATG TTG CTT GTC TGG TG and reverse primer 5′-GTC AGT CGA GTG CAC AGT TT. In addition, the Ptc-lacZ reporter mice, also known as $Ptch1^{D11}$ (26), were obtained from Cruris Inc. They were intercrossed with Nkx3.1Cre;$Klf6^{fl/fl}$ to produce the experimental cohorts. Mice were genotyped by PCR.

Prostate Microdissection, ex Vivo Three-dimensional Ultrasound, and ex Vivo Micro-CT—Prostates were harvested and treated with 1% collagenase (Sigma) for 15 min at 37 °C. Individual ducts were teased apart using forceps (11). A Leica Z6 APO microscope was used to acquire images of the microdissected prostates. Tissues were fixed in 4% paraformaldehyde. High resolution ultrasound imaging was employed to evaluate the interior of anterior prostate. The fixed tissue samples were placed in a bath of phosphate-buffered saline to provide acoustic coupling for *ex vivo* three-dimensional ultrasound micro-imaging. Ultrasound imaging was performed with a high resolution dedicated small animal ultrasound imaging system (Vevo 770, VisualSonics, Toronto, Canada). Images were acquired with a single-element (mechanical sweep) ultrasound transducer operating at a center frequency of 55 MHz and a 4.5 mm focal length, resulting in an axial resolution of 30 μm and a lateral resolution of 50 μm. Three-dimensional acquisition was performed by the linear translation of the transducer that was controlled by a motorized drive mechanism, where images were acquired every 50 μm to provide a three-dimensional field-of-view of $7 \times 7 \times 10$ mm. Images were processed with image analysis software provide with the Vevo 770 imaging.

Micro-CT was used to provide a quantitative analysis of the number of ductal tips and branch points. Microdissected tissues were soaked in 5% Isovue®/phosphate-buffered saline contrast agent for 2 h, blotted onto paper, and then suspended in soybean oil, which provides homogeneous and low x-ray absorption background for *ex vivo* micro-CT imaging. Samples were then imaged with the Scanco μCT40 (Bassendorf, Switzerland) micro-CT system at an isotropic voxel size of 12 μm. Images were acquired with the x-ray tube operating at an energy level of 45 kV and a current of 177 microamperes with an integration time of 300 ms. Acquired images were then analyzed using image analysis software from AnalyzeDirect (Lenexa, KS).

Histologic, Immunofluorescent Staining, and in Situ Hybridization Methods—We harvested prostate tissues from various genotypes and stages of development. Tissues for hematoxylin and eosin (H&E) histological staining purposes were formalin-fixed and paraffin embedded. Tissues were then sectioned and stained with H&E. Tissues for immunofluorescent staining were fixed in 4% paraformaldehyde/phosphate-buffered saline prior to Declere antigen retrieval (Cell Marque) using a pressure cooker for 10 min and then blocked in 10% donkey serum/phosphate-buffered saline. Primary antibodies used include rabbit anti-Klf6 (Santa Cruz Biotechnology, Santa Cruz, CA), rabbit anti-Ki67 (LabVision), rabbit anti-β-galactosidase (1:10,000, MP Biomedical, without antigen retrieval) (19), rabbit anti-androgen receptor (Upstate), rabbit anti-smooth muscle actin (LabVision), rabbit anti-desmin (EuroDiagnostica), rabbit anti-ck14 (Covance), mouse anti-ck8 (Novus), rabbit anti-phospho-Smad1/5/8 (1:500, Cell Signaling), and mouse anti-E-cadherin (BD Pharmingen). Secondary antibodies used to detect respective primary antibodies were anti-rabbit Alexa 488 (Invitrogen) and anti-mouse Alexa 594 (Invitrogen). Respective IgG controls were used on serial sections placed on each slide. Sections were mounted using Fluoromount containing 4′,6-diamidino-2-phenylindole stain (Dako).

Prostate tissues for non-radioactive *in situ* hybridization were harvested and fixed in 4% paraformaldehyde prior to embedding in an OCT compound and freezing on dry ice. Pretreatment of frozen tissue sections included proteinase K digestion (40 μg/ml, 6 min, and 25 °C) and acetylation (0.1 M triethanolamine, pH 8.0, 0.25% acetic anhydride, 10 min, 25 °C). Sections were hybridized with Riboprobes against Shh, Ptc, and Gli1 at 60 °C overnight, washed sequentially with 2× SSC, 1× SSC, 0.5× SSC, and blocked with 1× Digoxygenin-Block (Roche Applied Science) for 1 h before hybridization with alkaline phosphatase conjugated anti-Dig antibody (Roche Applied Science) for 1 h at room temperature.

Radioactive *in situ* hybridization was performed as previously described (27). PCR primers were designed to amplify a 415-bp fragment of mouse BMP4 spanning from nucleotides 948 to 1362 of mouse BMP4 reference sequence NM_007554.2 (upper, 5′-CAGGGCTTCCACCGTATAAAC-3′; lower, 5′-AATGGCGACGGCAGTT-3′). Primers included extensions encoding 27-nucletide T7 or T3 RNA polymerase initiation sites to allow *in vitro* transcription of sense or antisense probes, respectively, from the amplified products.

Formalin-fixed, paraffin-embedded sections 5-μm thick were deparaffinized, deproteinated in 10 μg/ml Proteinase K for 30 min at 37 °C, and further processed for *in situ* hybridization as previously described (Jubb *et al.* (27)). [^{33}P]UTP-labeled sense and antisense probes were hybridized to the sections at 55 °C overnight. Unhybridized probe was removed by incubation in 20 μg/ml RNase A for 30 min at 37 °C, followed by a high stringency wash at 55 °C in 0.1 × SSC for 2 h and dehydration through graded ethanols. The slides were dipped in NTB nuclear track emulsion (Eastman Kodak), exposed in sealed plastic slide boxes containing desiccant for 4 weeks at 4 °C, developed, and counterstained with H&E. Images were analyzed in Metamorph (version 7.0r4, MDS Analytical, Sunnyvale, CA). Briefly, regions of interest (epithelial ductal units)

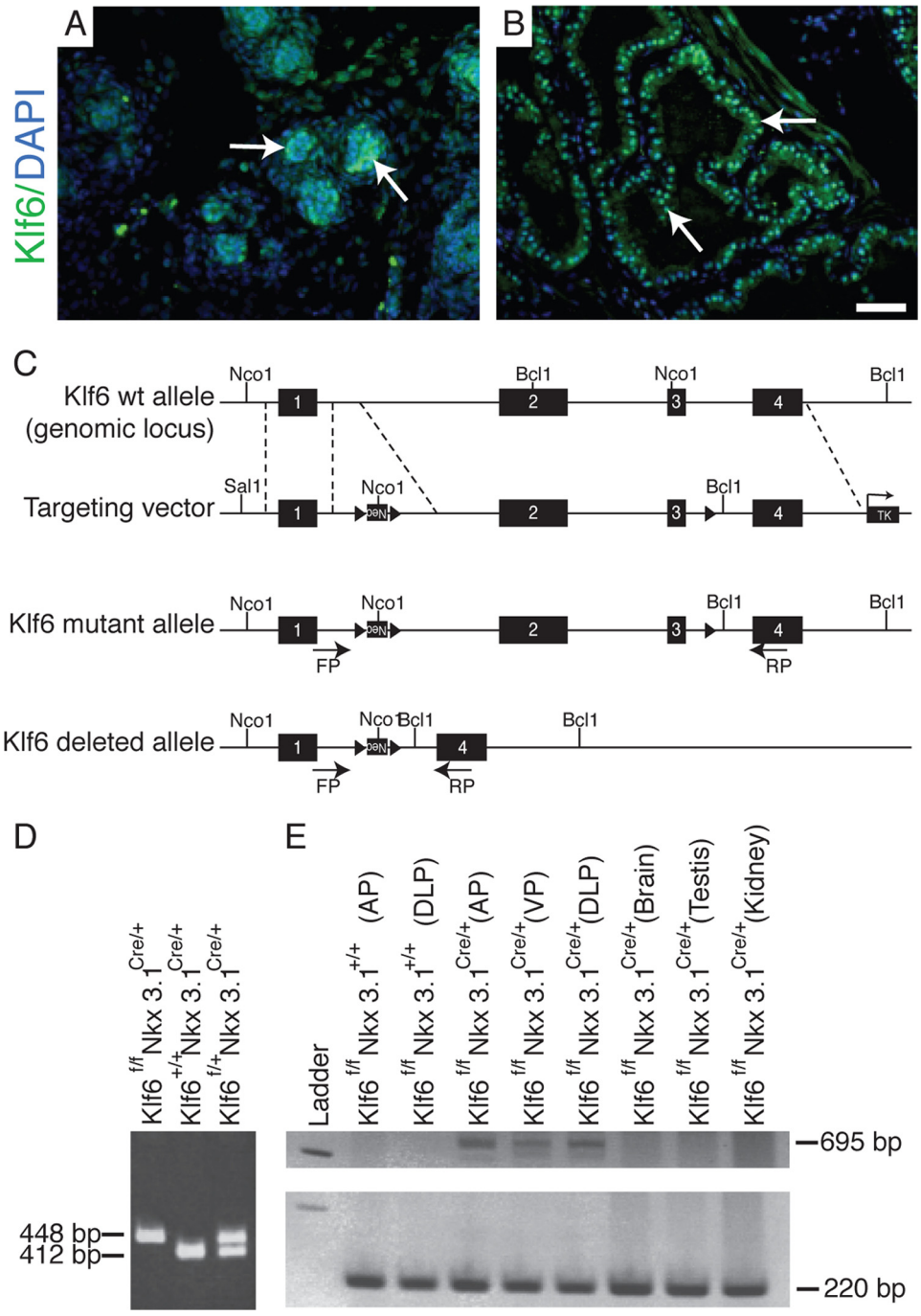

FIGURE 1. **Klf6 expression and generation of mutant mice with prostate-specific Klf6 deletion.** *A* and *B*, immunofluorescent staining of P4 and adult prostate, respectively, with anti-Klf6 revealed that nuclear Klf6 was expressed exclusively in the epithelial cells at both stages of development (*arrow*, *A* and *B*). Stromal staining was nonspecific and present in the anti-rabbit IgG control. *C*, a schematic drawing of the Klf6 wildtype (*wt*) genomic locus, targeting vector, *Klf6* floxed mutant allele (*Klf6*$^{f/f}$) and *Klf6* deleted allele upon Nkx3.1-driven Cre recombinase-mediated deletion. The targeting vector was generated by inserting two loxP sites flanking a *neo* cassette between exons 1 and 2 and a loxP site just upstream of exon 3. Cre recombination would result in the excision of exons 2 and 3. *D*, genotyping of Klf6 mutant mice by PCR analysis. PCR of genomic DNA from wild-type mice would yield a 412-bp band, and the Klf6$^{f/f}$ mice would yield a 448-bp PCR product due to the presence of a loxP site. *E*, reverse transcription-PCR analysis of mRNA obtained from anterior (*AP*), dorsolateral (*DLP*), and ventral (*VP*) prostate of Klf6$^{f/f}$ mice with and without Cre-recombinase and from the brain, testis, and kidney of Klf6$^{f/f}$Nkx3.1$^{Cre/+}$ tissues. Deletion of exons 2 and 3 from Klf6 would yield a 695-bp PCR product with the forward and reverse primer pair and equal loading was observed in all *lanes* through detection of a 220-bp PCR product of the *TCRD* gene. *Bar*, 50 μm for *A* and *B*.

were created manually to restrict analysis to the lumen. A threshold value was applied for each set of images (~95% of maximum pixel value) to identify positively stained areas. The total area of each region and the positive stained area for each region were outputted directly to Excel (Microsoft, Redmond, WA). A value of 10.3 pixels per silver grain was used to calculate the total number of silver grains associated with the positively stained area.

RESULTS

Generation of Mice with Prostate-specific Deletion of Klf6—To understand the developmental role of Klf6 in the prostate, we first defined the spatial and temporal expression pattern of Klf6. Anti-Klf6 immunofluorescent staining revealed that Klf6 expression was highly expressed in the nuclei of prostate epithelium as early as postnatal day 1 (P1) (data not shown), P4 (*arrow*, Fig. 1*A*), and mature prostate (*arrow*, Fig. 1*B*). The specificity of the anti-Klf6 antibody was confirmed by the lack of immunofluorescent staining in the nuclei of cells in which the *Klf6* were deleted (see below, Fig. 2, *N* and *P*).

To generate a prostate-specific deletion of exons 2 and 3 that encompass all three zinc fingers, which inactivates Klf6 transcription factor activity (Fig. 1*C*), we crossed Klf6 conditional mutant mice containing loxP sites flanking exons 2 and 3 (Klf6$^{f/f}$) with Nkx3.1$^{Cre/+}$ knock-in mice in which the Nkx3.1 promoter directs expression of Cre-recombinase to the prostate epithelium.[5] To demonstrate prostate-specific deletion of exons 2 and 3 from Klf6, we performed reverse transcription-PCR analysis on mRNA from various genotypes and tissues. A 695-bp PCR product, amplified when exons 2 and 3 were deleted, could only be detected in Klf6$^{f/f}$Nkx3.1 $^{Cre/+}$ prostate but not in brain, testes, and kidney or Klf6$^{f/f}$Nkx3.1$^{+/+}$ prostate. The highest level of Cre-mediated deletion of Klf6 was detected in the anterior prostate (Fig. 1*E*).

Branching and Canalization Defects in Klf6-deficient Prostate—Progression of prostate branching morphogenesis varies from lobe to lobe. Main ducts are present in all lobes at birth, but lateral branching in the ventral prostates begins at birth (P1), the ante-

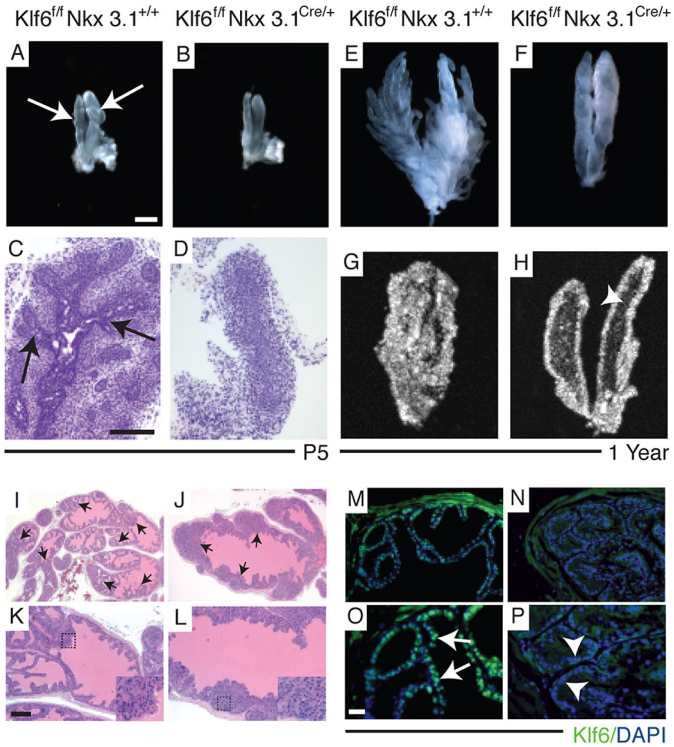

FIGURE 2. **Abnormality in ductal branching in the Klf6-deficient prostate epithelium.** Morphological ductal aberrations in Klf6-deficient anterior prostates were first observed at P5 and retained in adult mice. Light microscopy images (*A*, *B*, *E*, and *F*) and H&E staining (*C* and *D*) of Klf$^{f/f}$Nkx3.1$^{+/+}$ (*A*, *C*, and *E*) and Klf$^{f/f}$Nkx3.1$^{Cre/+}$ (*B*, *D*, and *F*) from P5 and 1-year-old anterior prostates that were microdissected prior to imaging. Only one side of the symmetrical anterior lobe was imaged, and three mice were imaged from each stage. Branching was visible in both microdissected (*arrow*, *A*) and H&E-stained (*arrow*, *C*) P5 sections from Klf$^{f/f}$Nkx3.1$^{+/+}$ but not in Klf$^{f/f}$Nkx3.1$^{Cre/+}$ (*B* and *D*). *Ex vivo* ultrasound imaging allowed visualization of the interior of anterior prostate of Klf$^{f/f}$Nkx3.1$^{+/+}$ (*G*) that appears dense and white due to extensive epithelial infolding in the ducts, and the single layer of while epithelial lumen that outlines the main ducts of Klf$^{f/f}$Nkx3.1$^{Cre/+}$ mice (*H*). *Arrowhead* (in *H*) points to the significantly enhanced luminal space present within the main duct of Klf$^{f/f}$Nkx3.1$^{Cre/+}$ anterior prostate. H&E staining of prostates obtained from 6-month-old (*I* and *K*) Klf$^{f/f}$Nkx3.1$^{+/+}$ and (*J* and *L*) Klf$^{f/f}$Nkx3.1$^{Cre/+}$ mice. Note that the widest region at the base of Klf$^{f/f}$Nkx3.1$^{+/+}$ prostate (*K*) fits into the field of view, whereas the narrowest region of Klf$^{f/f}$Nkx3.1$^{Cre/+}$ prostate (*L*) does not fit into the field of view. Epithelial infolding that spans the lumen was more extensive in Klf$^{f/f}$Nkx3.1$^{+/+}$ prostates (*arrow*, *I*) than Klf$^{f/f}$Nkx3.1$^{Cre/+}$ prostates (*arrow*, *J*). *Insets* represent higher magnification of the regions marked by the *dotted square* in *K* and *L*, respectively, that revealed nuclei with normal characteristics. Immunofluorescent staining of Klf6 expression in prostate tissues obtained from 8-week-old Klf$^{f/f}$Nkx3.1$^{+/+}$ (*M* and *O*) and Klf$^{f/f}$Nkx3.1$^{Cre/+}$ (*N* and *P*) mice. Klf6, which is a transcription factor, was highly localized to the nuclei of Klf$^{f/f}$Nkx3.1$^{+/+}$ prostate epithelium (*arrows*, *O*), and depletion of Klf6 in the Klf$^{f/f}$Nkx3.1$^{Cre/+}$ prostate was confirmed by the absence of green signal in the nuclei (*arrowhead*, *P*). *I*, *J*, *M*, and *N*, low magnification and high magnification (*K*, *L*, *O*, and *P*) of respective images. *Bar* in *A*, 500 μm for *A* and *B*, 1000 μm for *E* and *F*, and 750 μm for *G* and *H*. *Bar* in *C*, 50 μm for *C* and *D*. *Bar* in *K*, 200 μm for *I* and *J* and 100 μm for *K*–*N*. *Bar* in *O*, 50 μm for *O* and *P*.

rior prostate at P5, and the dorsolateral prostate by P10 (11, 28). Gross examination of all three lobes of Klf6$^{f/f}$Nkx3.1$^{Cre/+}$ prostates revealed a prominent branching phenotype primarily in the anterior prostate, which was consistent with the highest level of Klf6 depletion. The branching defect in the Klf6$^{f/f}$Nkx3.1$^{Cre/+}$ anterior prostates was evident as early as postnatal day 5 (P5) (Fig. 2, *B* and *D*). Impaired branching was 100% penetrant in the Klf6$^{f/f}$Nkx3.1$^{Cre/+}$ mice, whereas all Klf6$^{f/f}$Nkx3.1$^{+/+}$, Klf6$^{f/+}$Nkx3.1$^{Cre/+}$, and Klf6$^{+/+}$ Nkx3.1$^{Cre/+}$ prostates developed normally. To rule out a possibility of a delay in secondary branching, we examined Klf6$^{f/f}$ Nkx3.1$^{Cre/+}$ prostates from 6-month-old (data not shown) and 1-year-old (Fig. 2*F*) mice and found that those mature prostates were still without secondary branches as first noted at P5. This was in contrast to the extensive secondary and tertiary branching observed in 1-year-old Klf6$^{f/f}$Nkx3.1$^{+/+}$ mice (Fig. 2*E*). Distinguishing branching features in the dorsal and ventral prostates were not as apparent between Klf6$^{f/f}$Nkx3.1$^{+/+}$ and Klf6$^{f/f}$Nkx3.1$^{Cre/+}$ except for larger luminal spaces in the ducts (supplemental Fig. S1, *A*–*D*). This milder phenotype could be due to less efficient Klf6 deletion in those lobes, because the greatest level of Klf6 deletion was primarily in the anterior lobe, the remainder of our analyses focused therefore on detailed characterization of the anterior prostate.

Canalization of the anterior prostate begins around P2 and progresses in a proximal to distal manner with elaboration of epithelial infolding or tufting within the luminal space (28, 29). A novel *ex vivo* application of three-dimensional, high resolution ultrasound micro-imaging technology was employed to visualize the luminal space of intricately microdissected prostates. Extensive epithelial infolding in the smaller luminal space of 1-year-old Klf6$^{f/f}$Nkx3.1$^{+/+}$ anterior prostates resulted in a dense, white, hyperechoic regions within the ultrasound image (Fig. 2*G*), which were also visible by H&E staining (Fig. 2, *I* and *K*). The absence of secondary branching from the two main ducts was evident in the Klf6$^{f/f}$Nkx3.1$^{Cre/+}$ anterior prostates (Fig. 2*H*). *Ex vivo* ultrasound imaging revealed a dark, hypoechoic luminal space in the main ducts, suggesting that canalization was unaffected (*arrowhead*, Fig. 2*H*). The epithelial infolding in the Klf6$^{f/f}$Nkx3.1$^{Cre/+}$ anterior prostate was significantly reduced resulting in a defined layer of epithelial cells outlining the main ducts (Fig. 2*H*). H&E-stained sections also revealed that the epithelial infolding rarely spanned across the lumen, and the eosinophilic lumen suggests a functional epithelium, capable of secretion (Fig. 2, *J* and *L*). Further histopathological analysis of the H&E-stained Klf6$^{f/f}$Nkx3.1$^{Cre/+}$ sections did not reveal any signs of hyperproliferation, nuclear anomalies, or mitotic figures (*insets*, Fig. 2, *J* and *L*). Given the normal appearance of the luminal epithelium, we performed anti-Klf6 immunofluorescent staining to confirm that Klf6 protein was indeed depleted in the prostate epithelium. In Klf6$^{f/f}$Nkx3.1$^{+/+}$ mice, nuclear Klf6 expression was detected in the prostate epithelium (*arrow*, Fig. 2*O*), whereas positive nuclear staining was absent from Klf6$^{f/f}$Nkx3.1$^{Cre/+}$ epithelium (*arrowhead*, Fig. 2*P*).

To quantify the number of ductal tips and branch points we used *ex vivo* micro-CT to image the anterior prostate. It was necessary to microdissect away connective tissues encapsulating the prostate to reveal adequately separated ducts ideal for micro-CT imaging. We found significantly ($p < 0.001$) more ductal tips (*red dot*) and branch points (*red Y*) in the anterior prostate of Klf6$^{f/f}$Nkx3.1$^{+/+}$ mice (Fig. 3, *A*, *C*, and *E*) than Klf6$^{f/f}$Nkx3.1$^{Cre/+}$ mice (Fig. 3, *B*, *D*, and *F*). It should be pointed out that, although Nkx3.1 null mice show a defect in prostatic branching morphogenesis (25, 30), the ductal epithelium in Nkx3.1$^{+/-}$ mice is essentially indistinguishable from wild type at 2 months of age and only shows much milder phenotype than that in Nkx3.1$^{-/-}$ mice at an age of 10–12 months

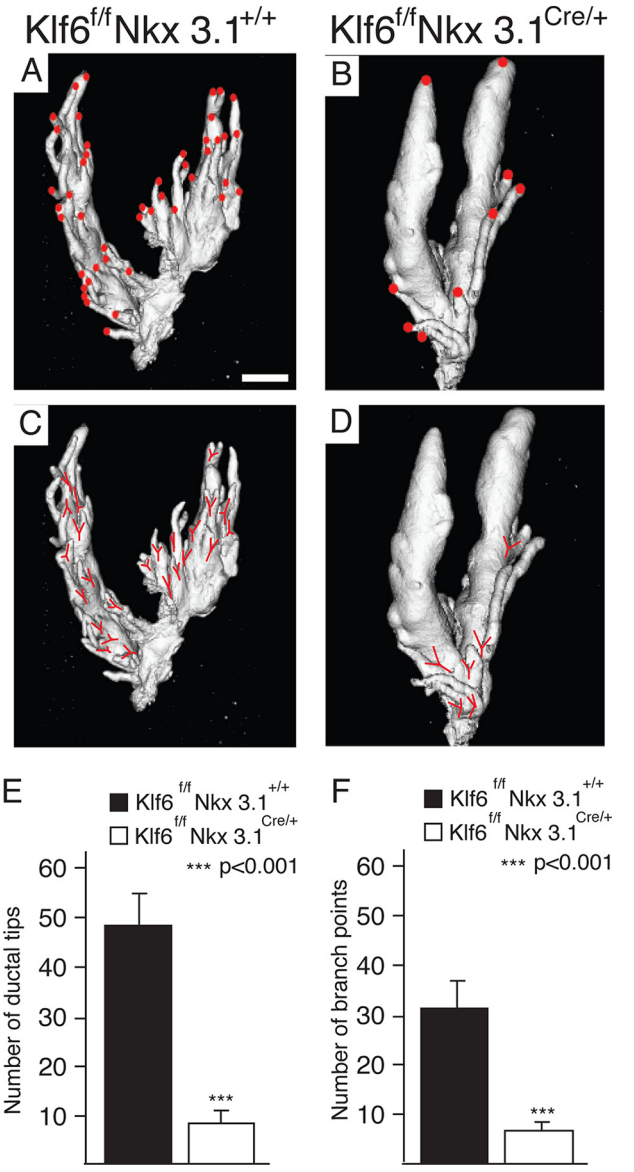

FIGURE 3. **Impaired lateral branching in Klf6-deficient anterior prostates.** Microdissected prostate from Klf$^{f/f}$Nkx3.1$^{+/+}$ (*A* and *C*) and Klf$^{f/f}$Nkx3.1$^{Cre/+}$ (*B* and *D*) mice were imaged using *ex vivo* micro-CT and three-dimensional images were reconstructed. Ductal tips (*A* and *B*) and branch points (*C* and *D*) were marked on the three-dimensional images, counted ($n = 4$ from each genotype) and plotted in *bar graphs*, respectively (*E* and *F*). The number of ductal tips and branch points sprouting out of the main ducts are significantly more in (*A*, *C*, and *E*) Klf$^{f/f}$Nkx3.1$^{+/+}$ than (*B*, *D*, and *F*) Klf$^{f/f}$Nkx3.1$^{Cre/+}$ prostates. Statistical significance was calculated using Student's *t* test, and the *bars* represent mean ± S.E. *Bar*, 1 mm for *A–D*.

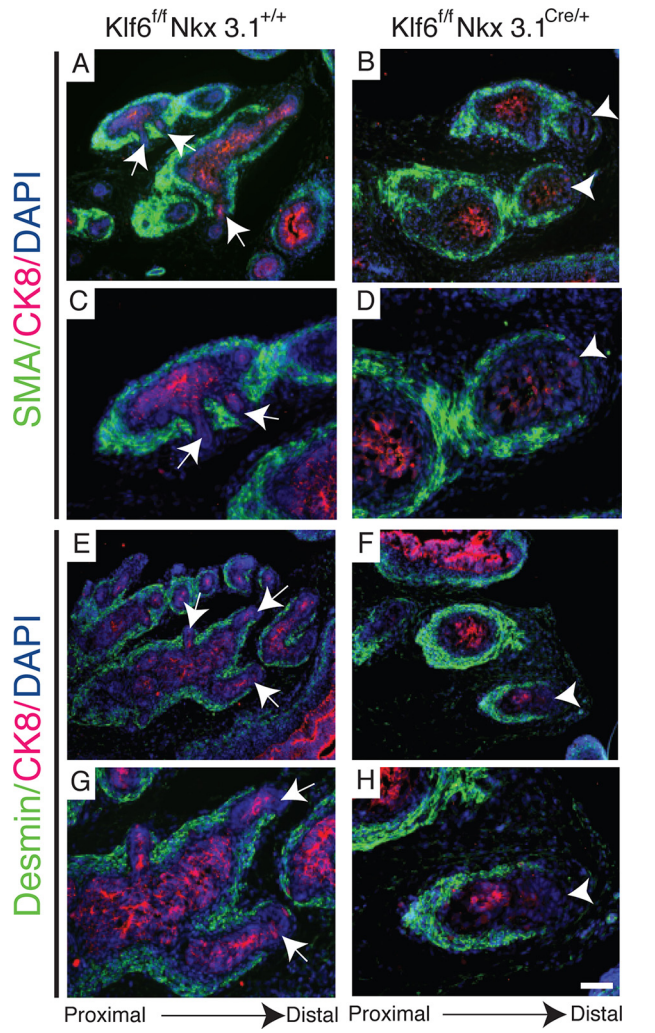

FIGURE 4. **Smooth muscle formed along the sides of Klf6-deficient main ducts of the anterior prostate without intermittent smooth muscle deficient areas to permit lateral branching.** Immunofluorescent staining of P5 Klf$^{f/f}$Nkx3.1$^{+/+}$ anterior prostates showed similar expression of early smooth muscle marker, SMA and late marker (*A* and *C*), desmin lining the ducts (*E* and *G*) but absent in areas where new lateral branches were formed (*arrow*). In Klf$^{f/f}$Nkx3.1$^{Cre/+}$ anterior prostates, SMA (*B* and *D*) and desmin (*F* and *H*) were expressed continuously along the entire length of the main ducts except for the distal tip (*arrowhead*). Low magnification (*A*, *B*, *E*, and *F*) and high magnification (*C*, *D*, *G*, and *H*) of respective images. *Bar*, 100 μm for *A*, *B*, *E*, and *F*, and 50 μm for *C*, *D*, *G*, and *H*.

or older (Fig. 4*E* of (30)). The branching defect due to conditional Klf6 deletion reported in the present study is far more severe than that found even in Nkx3.1 homozygous knockouts (Figs. 2*F* and 3 of the present study, as compared with Fig. 4 (*I* and *J*) of Ref. 25). These findings together argue strongly that Klf6 inactivation makes important contribution to the defect in prostate branching morphogenesis.

Characterization of Gene Expression in Abnormal Prostate Resulting from Loss of Klf6—Murine prostate development begins in late gestation, in a process involving reciprocal interactions between the prostate epithelium and mesenchyme (31, 32). During development, the mesenchyme condenses around the ducts in a proximal to distal fashion to encase the ducts with smooth muscle actin (SMA), the earliest smooth muscle marker expressed, and desmin, a later marker (33). To determine the state of smooth muscle differentiation, we examined the expression of SMA and desmin at P5, which corresponds to the initiation of secondary branching in the anterior prostate. We found SMA (Fig. 4, *A* and *C*) and desmin (Fig. 4, *E* and *G*) expressed proximally but not at the distal tips (*arrow*) of newly branched lateral ducts of Klf6$^{f/f}$Nkx3.1$^{+/+}$ prostates. In contrast, SMA (Fig. 4, *B* and *D*) and desmin (Fig. 4, *F* and *H*) were expressed along the entire length of each main duct of Klf6$^{f/f}$ Nkx3.1$^{Cre/+}$, but not at the distal tip (*arrowhead*). Interestingly, this is consistent with previous findings where the relative thickness of the smooth muscle layer is inversely proportional to epithelial ductal growth (34). This suggests that, although there was diminished *smooth* muscle expression around the

emerging lateral ducts of Klf6$^{f/f}$Nkx3.1$^{+/+}$ prostates, lateral epithelial branching in Klf6$^{f/f}$Nkx3.1$^{Cre/+}$ was prevented as a result of a continuous layer of smooth muscle along the main ducts. On the other hand, it is also possible that the continuous layer of smooth muscle formed around the main ducts as a result of the absence of branching. To further understand this branching defect, we examined expression of androgen receptor by immunofluorescent staining, because several investigators had demonstrated that postnatal prostate branching morphogenesis and differentiation of the stroma are highly regulated by androgen (32, 33, 35). Androgen receptor was expressed continuously around the primary and secondary ducts of Klf6$^{f/f}$Nkx3.1$^{+/+}$ (supplemental Fig. S2, *A* and *C*) and the main ducts of Klf6$^{f/f}$Nkx3.1$^{Cre/+}$ prostates (supplemental Fig. S2, *B* and *D*). There were no apparent differences in proliferation by anti-Ki67 staining (supplemental Fig. S3, *A* and *B*), cell death by anti-active caspase-3 (data not shown) and epithelial differentiation by anti-CK8, anti-CK14 and anti-E-cadherin staining (supplemental Figs. S2 (*E–H*) and S3 (*C* and *D*)). Therefore, the lack of lateral branching could not be attributed to androgen receptor expression, proliferation, cell death, or epithelial differentiation in the mutant mice.

Factors in the epithelium and mesenchyme essential for proper ductal branching include Nkx3.1, Hh, BMP, FGF, Notch, and Wnt pathway components (12–19, 25, 36). Our group and others have previously shown that the activated Shh pathway could inhibit prostatic ductal branching (12–15, 37). The lack of branching in the Klf6$^{f/f}$Nkx3.1$^{Cre/+}$ prostates prompted us to examine mRNA expression of Shh pathway components by *in situ* hybridization. In Klf6$^{f/f}$Nkx3.1$^{+/+}$ prostates, highly localized epithelial Shh expression was detected in the distal tips, which was consistent with a previous reported study (37) (*arrow*, Fig. 5, *A* and *C*). However, Shh expression was dispersed throughout the entire length of the Klf6$^{f/f}$Nkx3.1$^{Cre/+}$ main ducts (Fig. 5, *B* and *D*). Similarly, intense and dispersed expression of Ptc and Gli1, two well validated Hh target genes (38, 39), were detected throughout the stroma surrounding the main ducts of Klf6$^{f/f}$Nkx3.1$^{Cre/+}$ (*arrowhead*, Fig. 5, *F* and *J*). This was in sharp contrast to the highly localized expression of Ptc and Gli1 observed in the stroma adjacent to Shh expression in the ductal tips of Klf6$^{f/f}$Nkx3.1$^{+/+}$ that was previously shown in wild-type prostates (37) (*arrow*, Fig. 5, *E*, *G*, *I*, and *K*).

To confirm the change in expression pattern of Ptc, we crossed Klf6$^{f/+}$Nkx3.1$^{Cre/+}$ with Ptc-lacZ reporter mice (26) in which lacZ is driven under the Pct promoter, to obtain Klf6$^{f/f}$Nkx3.1$^{Cre/+}$;Ptc-lacZ mice. This Ptc-lacZ reporter line is a well characterized and a sensitive indicator of endogenous Ptc expression or Hh signaling activity (26). Consistent with the *in situ* hybridization results, we found that there was increased β-galactosidase staining in the periepithelial stoma of Klf6$^{f/f}$Nkx3.1$^{Cre/+}$;Ptc-lacZ mice compared with the staining observed in Klf6$^{f/f}$Nkx3.1$^{+/+}$;Ptc-lacZ mice (Fig. 6). There were multiple cell layers of β-galactosidase-positive cells surrounding the epithelium in the Klf6$^{f/f}$Nkx3.1$^{Cre/+}$;Ptc-lacZ mice (Fig. 6, *A* and *C*). In sharp contrast, only one to two layers of β-galactosidase-positive cells were seen in the Klf6$^{f/f}$Nkx3.1$^{+/+}$; Ptc-lacZ control littermates (Fig. 6, *B* and *D*). Together these findings indicate that Klf6 expression leads to broader expression of Hh signaling around the developing prostate ducts.

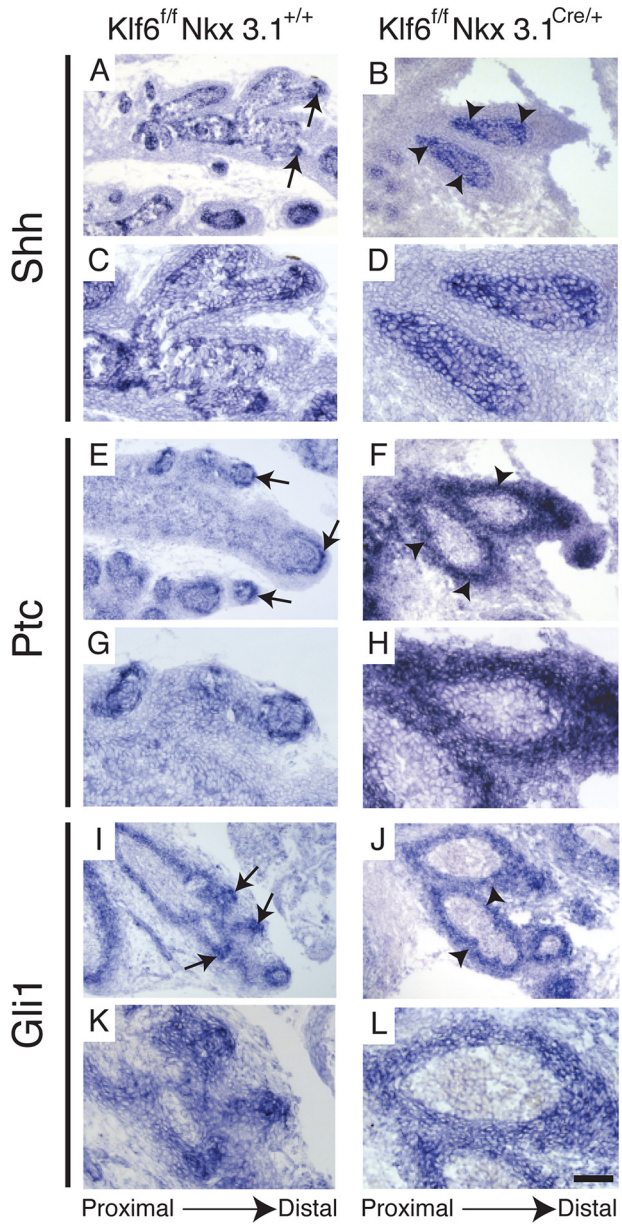

FIGURE 5. **Enhanced expression of Shh pathway components in Klf6-deficient prostate.** *In situ* hybridization analysis of P7 Klf$^{f/f}$Nkx3.1$^{+/+}$ prostates revealed expression of Shh in the epithelium at the tips of lateral branches (*arrow*, *A*). Shh expression was elevated and dispersed throughout the main ductal epithelium of Klf$^{f/f}$Nkx3.1$^{Cre/+}$ prostates (*arrowhead*, *B*). Localized Ptc (*arrow*, *E* and *G*) and Gli1 (*arrow*, *I* and *K*) expression in Klf$^{f/f}$Nkx3.1$^{+/+}$ prostates were detected in the stromal region immediately adjacent to the Shh expressing epithelium at the ductal tips. However, in the Klf$^{f/f}$Nkx3.1$^{Cre/+}$ prostates, Ptc (*arrowhead*, *F* and *H*) and Gli1 (*arrowhead*, *J* and *L*) expression were highly elevated and localized expression to the stroma at the ductal tips was lost. Instead, Ptc and Gli expression were dispersed throughout the perimeter of the main ducts (*arrowhead*, *F*, *H*, *J*, and *L*). Low magnification (*A*, *B*, *E*, *F*, *I*, and *G*) and high magnification (*C*, *D*, *G*, *H*, *K*, and *L*) of respective images. *Bars*: 100 μm for *A*, *B*, *E*, *F*, *I*, and *G*, and 50 μm for *C*, *D*, *G*, *H*, and *K*.

In an attempt to further understand how epithelial branching morphogenesis is inhibited in the Klf6$^{f/f}$Nkx3.1$^{Cre/+}$ mice, we also performed radioactive *in situ* hybridization using a probe specific for BMP4, which was previously shown to be expressed in the prostatic stroma and can inhibit prostatic epithelial duc-

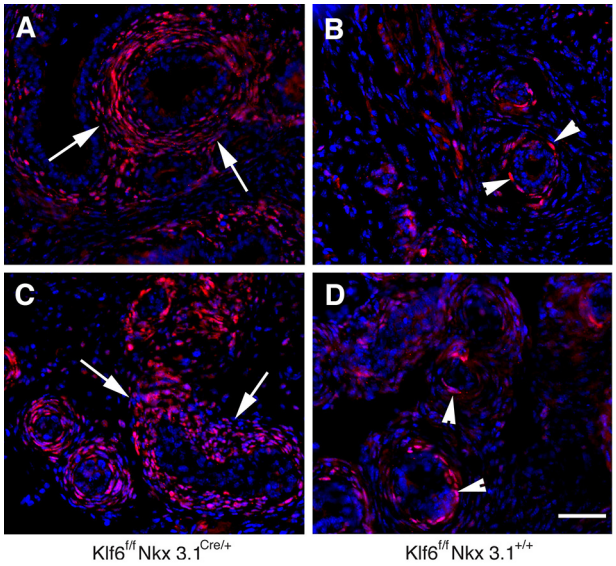

FIGURE 6. **β-Galactosidase expression in Klf6$^{f/f}$Nkx3.1$^{Cre/+}$;Ptc-lacZ reporter mouse prostates.** Immunostaining of prostate tissue sections prepared from P7 Klf6$^{f/f}$Nkx3.1$^{Cre/+}$;Ptc-lacZ (*A* and *C*) and Klf6$^{f/f}$Nkx3.1$^{+/+}$;Ptc-lacZ (*B* and *D*) mice with anti-β-galactosidase antibody. The sections were counterstaining with 4′,6-diamidino-2-phenylindole (*blue*). Note that β-galactosidase-expressing cells are located in the mesenchymal cells surrounding the epithelium. Although there were multiple cell layers of β-galactosidase positive cells in the Klf6$^{f/f}$Nkx3.1$^{Cre/+}$;Ptc-lacZ mice (*A* and *C*), only one to two layers of β-galactosidase-positive cells were seen in the Klf6$^{f/f}$Nkx3.1$^{+/+}$; Ptc-lacZ control littermates. Slides were viewed using a Zeiss Axiophot epifluorescence microscope. Images were captured with Compix imaging systems using a cooled RGB charge-coupled device camera and analyzed using Adobe Photoshop CS. *Bar*, 50 μm.

tal budding and branching morphogenesis (17). As shown in Fig. 7, which contains tangential sections of P7 prostates, overall expression of BMP4 in the stroma surrounding the epithelium was enhanced in Klf6$^{f/f}$Nkx3.1$^{Cre/+}$ mice (Fig. 7, *A–D*) compared with the expression levels observe in sections taken from Klf6$^{f/f}$ Nkx3.1$^{+/+}$ mice (Fig. 7, *E–H*). Upon quantification of the silver grains from the *in situ* hybridization, there was more than 4-fold BMP4 expression in the Klf6$^{f/f}$Nkx3.1$^{Cre/+}$ mice as compared with the Klf6$^{f/f}$Nkx3.1$^{+/+}$ mice ($p < 0.05$, Fig. 7*I*). Next, we investigated the status of signaling downstream of BMP4 by examining the phosphorylation status of Smad1/5/8. Immunofluorescence staining using anti-phospho-Smad1/5/8 antibody revealed enhanced nuclear staining in the prostate sections from Klf6$^{f/f}$Nkx3.1$^{Cre/+}$ mice, whereas there were only a few positively stained nuclei in the Klf6$^{f/f}$Nkx3.1$^{+/+}$ sections (Fig. 7, *J* and *K*). These findings together suggest that up-regulation of Hh signaling induced by the deletion of the Klf6 gene may inhibit prostate epithelial branching via up-regulation of BMP4.

DISCUSSION

The *Klf* gene family is known to be crucial for development in vertebrates (4). They are expressed in a large number of tissues (40) and play an important role in the control of hematopoietic cell differentiation (4), erythroid cell maturation (21, 41), T-cell activation (42), blood vessel stability (20), and skin permeability (22). Using the prostate as a model, we describe here for the first time a role for Klf6 in prostate branching morphogenesis. Consistent with this notion, Klf14, another Klf family member, has been shown to be critical for alveolarization in the developing lung. Deletion of Klf14 leads to thinner lung alveolar walls and poor outgrowth of secondary septa, which results in defective blood-air exchange and respiratory failures in newborn mice (43). In the kidney, Klf6 is known to be expressed in the Wolffian duct, uteric bud, collecting ducts, and mesangium (44), an expression profile that would also be consistent with a role in branching morphogenesis.

Because systemic loss of Klf6 is embryonic lethal (23), we generated mice deficient for Klf6 specifically in the prostate. The resulting lateral branching defect in Klf6-deficient prostate was confirmed by light microscopy, H&E staining, and micro-CT imaging. Using a novel *ex vivo* ultrasound imaging modality, we were able to demonstrate that Klf6 plays a role in modulating the epithelial infolding and tufting, which results in decreased surface area of functional epithelium. The most prominent branching defects are seen in the anterior prostate, also known as a coagulating gland, which correlates with the highest level of Klf6 depletion (Fig. 1*E*). Despite the reduction in epithelial infolding and tufting whether or not prostatic function has been impaired in these mice remains to be determined.

The augmented branching defect in the anterior prostate is noteworthy, because the branching patterns in the anterior prostate are distinct from the dorsolateral prostate and ventral prostate. In addition, the embryologic origin of the anterior prostate is also different from the other prostate lobes (45, 46). Although branching patterns of the ventral prostate and dorsolateral prostates are believed to arise from the urogenital sinus epithelium invaginating into urogenital sinus mesenchyme, the anterior prostate is thought to be derived from urogenital sinus epithelium at the most dorsal aspect of the urogenital sinus invaginating into the mesenchyme of the seminal vesicle, which itself is derived from the mesodermal Wolffian duct. Hence, the resulting branched structure in the anterior prostate has unique patterns distinct from the other prostate lobes and occurs as a result of lateral branch events and not as a result of bifurcations at the elongating tips.

Consistent with previous reports from our group and others on the role of Shh signaling in prostate branching (12–15, 37), both Ptc-lacZ reporter mice crossed to Klf6$^{f/f}$Nkx3.1$^{Cre/+}$ mice and *in situ* hybridization data in the present study indicate that impaired lateral branching in the Klf6-deficient prostate correlate with an up-regulation and loss of spatial localization of Shh, Ptc, and Gli1. Further support for the involvement of focal Hh signaling in prostate epithelial branching comes from a study by Bushman and co-workers (15), showing a close association between prostate ductal bud formation and localized expression of Shh at the growing tips of elongating prostate ducts. In addition, Shh regulates prostate branching morphogenesis in concert with FGF10 and BMP4 (37). Shh secreted from the epithelial ductal tips can down-regulate FGF10 that stimulates epithelial cell growth (16) and/or up-regulate BMP4 that inhibits epithelial cell growth (17) in the mesenchyme, which results in epithelial ductal branching (37). In the present study, we show that loss of Klf6 leads to dispersed, rather than focal, Shh expression throughout the epithelial ducts and corresponding dispersed Ptc and Gli1 expression in the adjacent mesenchyme (Fig. 5). This broader domain of Hh pathway activity leads to an up-regulation of BMP4 expres-

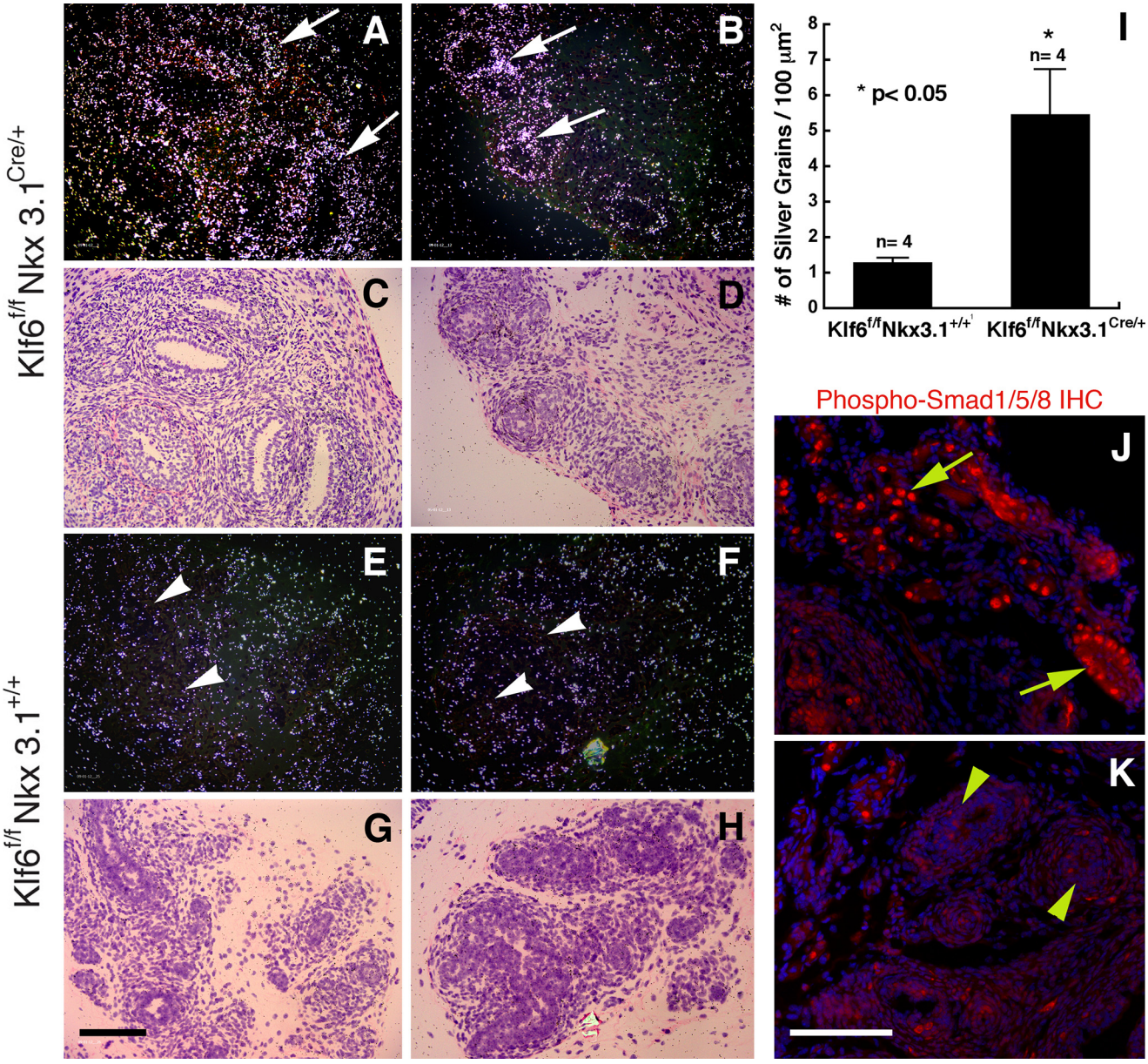

FIGURE 7. **Expression of BMP4 is up-regulated in Klf6$^{f/f}$Nkx3.1$^{Cre/+}$ mice.** *A* and *B*, BMP4 expression detected by radioactive *in situ* hybridization in P7 Klf6$^{f/f}$Nkx3.1$^{Cre/+}$ prostates. *C* and *D*, H&E staining from the same field of *A* and *B*. *E* and *F*, BMP4 expression in P7 Klf6$^{f/f}$Nkx3.1$^{+/+}$ prostates. *G* and *H*, H&E staining from the same field of *E* and *F*. Note that the BMP4 signal is stronger and broader in the mutants compared with the control mice (*arrows* in *A* and *B versus arrowheads* in *E* and *F*). *I*, MetaMorph analysis of numbers of silver grains per μm^2 indicates a significant increase in the prostate of Klf6$^{f/f}$Nkx3.1$^{Cre/+}$ mice as compared with that of Klf6$^{f/f}$Nkx3.1$^{+/+}$ mice. Sense control probes revealed no hybridization signal above background (not shown). *J* and *K*, phospho-Smad1/5/8 immunostaining of P7 prostates from Klf6$^{f/f}$Nkx3.1$^{Cre/+}$ and Klf6$^{f/f}$Nkx3.1$^{+/+}$ mice. Note that the staining is stronger, and the number of phospho-Smad1/5/8-positive nuclei is higher in the Klf6$^{f/f}$Nkx3.1$^{Cre/+}$ prostate (*yellow arrows* in *J*) than the Klf6$^{f/f}$Nkx3.1$^{+/+}$ prostate (*yellow arrowheads* in *K*). *Bar* in *G*, 100 μm for *A–H*; *bar* in *K*, 100 μm for *J* and *K*.

sion, resulting in reduced ductal branching. As proposed by Pu and coworkers, the interplay and localized expression pattern of Shh and BMP4 are key to conveying critical branching information (37).

Klf6 is reported to be a tumor suppressor that is inactivated in a large subset of prostate cancer (47). However, our detailed histological characterization of Klf6$^{f/f}$Nkx3.1$^{+/+}$ mice as old as 2 years failed to reveal any prostate tumors.[7] The lack of tumor phenotype in the Klf6 mutant mice could be due to compensations/redundancy with other Klf family members. It is also possible that loss of Klf6 might not be sufficient to initiate prostate tumorigenesis in the mouse and that loss/mutation of additional tumor suppressors might be required.

Acknowledgments—We thank Leisa Johnson, Mallika Singh, Hua Tian, and Zhenyu Gu for critical discussions. We also thank Margaret Fuentes, Christine Olsson, and Luz Orellana for assistance with the animal colony, Allison Bruce with Graphics, Jeffrey Eastham-Anderson for Metamorph analysis of BMP4 in situ hybridization signal, and Howard Stern for his assistance with some histopathological review.

[7] C. C. Leow, B. Wang, J. Ross, S. M. Chan, J. Zha, R. A. D. Carano, G. Frantz, M. M. Shen, F. J. de Sauvage, and W.-Q. Gao, unpublished observations.

REFERENCES

1. Bieker, J. J. (2001) *J. Biol. Chem.* **276,** 34355–34358
2. Huber, T. L., Perkins, A. C., Deconinck, A. E., Chan, F. Y., Mead, P. E., and Zon, L. I. (2001) *Curr. Biol.* **11,** 1456–1461
3. Laub, F., Aldabe, R., Friedrich, V., Jr., Ohnishi, S., Yoshida, T., and Ramirez, F. (2001) *Dev. Biol.* **233,** 305–318
4. Oates, A. C., Pratt, S. J., Vail, B., Yan, Y. I., Ho, R. K., Johnson, S. L., Postlethwait, J. H., and Zon, L. I. (2001) *Blood* **98,** 1792–1801
5. Zhao, W., Hisamuddin, I. M., Nandan, M. O., Babbin, B. A., Lamb, N. E., and Yang, V. W. (2004) *Oncogene* **23,** 395–402
6. Chen, C., Bhalala, H. V., Qiao, H., and Dong, J. T. (2002) *Oncogene* **21,** 6567–6572
7. Narla, G., Heath, K. E., Reeves, H. L., Li, D., Giono, L. E., Kimmelman, A. C., Glucksman, M. J., Narla, J., Eng, F. J., Chan, A. M., Ferrari, A. C., Martignetti, J. A., and Friedman, S. L. (2001) *Science* **294,** 2563–2566
8. Reeves, H. L., Narla, G., Ogunbiyi, O., Haq, A. I., Katz, A., Benzeno, S., Hod, E., Harpaz, N., Goldberg, S., Tal-Kremer, S., Eng, F. J., Arthur, M. J., Martignetti, J. A., and Friedman, S. L. (2004) *Gastroenterology* **126,** 1090–1103
9. Kimmelman, A. C., Qiao, R. F., Narla, G., Banno, A., Lau, N., Bos, P. D., Nuñez Rodriguez, N., Liang, B. C., Guha, A., Martignetti, J. A., Friedman, S. L., and Chan, A. M. (2004) *Oncogene* **23,** 5077–5083
10. Ito, G., Uchiyama, M., Kondo, M., Mori, S., Usami, N., Maeda, O., Kawabe, T., Hasegawa, Y., Shimokata, K., and Sekido, Y. (2004) *Cancer Res.* **64,** 3838–3843
11. Sugimura, Y., Cunha, G. R., and Donjacour, A. A. (1986) *Biol. Reprod.* **34,** 961–971
12. Freestone, S. H., Marker, P., Grace, O. C., Tomlinson, D. C., Cunha, G. R., Harnden, P., and Thomson, A. A. (2003) *Dev. Biol.* **264,** 352–362
13. Wang, B. E., Shou, J., Ross, S., Koeppen, H., De Sauvage, F. J., and Gao, W. Q. (2003) *J. Biol. Chem.* **278,** 18506–18513
14. Berman, D. M., Desai, N., Wang, X., Karhadkar, S. S., Reynon, M., Abate-Shen, C., Beachy, P. A., and Shen, M. M. (2004) *Dev. Biol.* **267,** 387–398
15. Lamm, M. L., Catbagan, W. S., Laciak, R. J., Barnett, D. H., Hebner, C. M., Gaffield, W., Walterhouse, D., Iannaccone, P., and Bushman, W. (2002) *Dev. Biol.* **249,** 349–366
16. Thomson, A. A., and Cunha, G. R. (1999) *Development* **126,** 3693–3701
17. Lamm, M. L., Podlasek, C. A., Barnett, D. H., Lee, J., Clemens, J. Q., Hebner, C. M., and Bushman, W. (2001) *Dev. Biol.* **232,** 301–314
18. Wang, X. D., Leow, C. C., Zha, J., Tang, Z., Modrusan, Z., Radtke, F., Aguet, M., de Sauvage, F. J., and Gao, W. Q. (2006) *Dev. Biol.* **290,** 66–80
19. Wang, B. E., Wang, X. D., Ernst, J. A., Polakis, P., and Gao, W. Q. (2008) *PLoS ONE* **3,** e2186
20. Kuo, C. T., Veselits, M. L., Barton, K. P., Lu, M. M., Clendenin, C., and Leiden, J. M. (1997) *Genes Dev.* **11,** 2996–3006
21. Nuez, B., Michalovich, D., Bygrave, A., Ploemacher, R., and Grosveld, F. (1995) *Nature* **375,** 316–318
22. Segre, J. A., Bauer, C., and Fuchs, E. (1999) *Nat. Genet.* **22,** 356–360
23. Matsumoto, N., Kubo, A., Liu, H., Akita, K., Laub, F., Ramirez, F., Keller, G., and Friedman, S. L. (2006) *Blood* **107,** 1357–1365
24. Deleted in proof
25. Bhatia-Gaur, R., Donjacour, A. A., Sciavolino, P. J., Kim, M., Desai, N., Young, P., Norton, C. R., Gridley, T., Cardiff, R. D., Cunha, G. R., Abate-Shen, C., and Shen, M. M. (1999) *Genes Dev.* **13,** 966–977
26. Oro, A. E., and Higgins, K. (2003) *Dev. Biol.* **255,** 238–248
27. Jubb, A. M., Pham, T. Q., Frantz, G. D., Peale, F. V. Jr., and Hillan, K. J. (2006) *Methods Mol Biol.* **326,** 255–264
28. Lung, B., and Cunha, G. R. (1981) *Anat. Rec.* **199,** 73–88
29. Shappell, S. B., Thomas, G. V., Roberts, R. L., Herbert, R., Ittmann, M. M., Rubin, M. A., Humphrey, P. A., Sundberg, J. P., Rozengurt, N., Barrios, R., Ward, J. M., and Cardiff, R. D. (2004) *Cancer Res.* **64,** 2270–2305
30. Schneider, A., Brand, T., Zweigerdt, R., and Arnold, H. (2000) *Mech. Dev.* **95,** 163–174
31. Cunha, G. R., and Donjacour, A. (1987) *Prog. Clin. Biol. Res.* **239,** 273–282
32. Cunha, G. R. (1994) *Cancer* **74,** 1030–1044
33. Hayward, S. W., Baskin, L. S., Haughney, P. C., Foster, B. A., Cunha, A. R., Dahiya, R., Prins, G. S., and Cunha, G. R. (1996) *Acta Anat.* (*Basel*) **155,** 94–103
34. Nemeth, J. A., and Lee, C. (1996) *Prostate* **28,** 124–128
35. Donjacour, A. A., and Cunha, G. R. (1993) *Endocrinology* **132,** 2342–2350
36. Tanaka, M., Komuro, I., Inagaki, H., Jenkins, N. A., Copeland, N. G., and Izumo, S. (2000) *Dev. Dyn.* **219,** 248–260
37. Pu, Y., Huang, L., and Prins, G. S. (2004) *Dev. Biol.* **273,** 257–275
38. Ramalho-Santos, M., Melton, D. A., and McMahon, A. P. (2000) *Development* **127,** 2763–2772
39. Madison, B. B., Braunstein, K., Kuizon, E., Portman, K., Qiao, X. T., and Gumucio, D. L. (2005) *Development* **132,** 279–289
40. Turner, J., and Crossley, M. (1999) *Trends Biochem. Sci.* **24,** 236–240
41. Perkins, A. C., Gaensler, K. M., and Orkin, S. H. (1996) *Proc. Natl. Acad. Sci. U.S.A.* **93,** 12267–12271
42. Kuo, C. T., Veselits, M. L., and Leiden, J. M. (1997) *Science* **277,** 1986–1990
43. Hertveldt, V., Louryan, S., van Reeth, T., Drèze, P., van Vooren, P., Szpirer, J., and Szpirer, C. (2008) *Dev. Dyn.* **237,** 883–892
44. Fischer, E. A., Verpont, M. C., Garrett-Sinha, L. A., Ronco, P. M., and Rossert, J. A. (2001) *J. Am Soc. Nephrol.* **12,** 726–735
45. Cunha, G. R., and Lung, B. (1979) in *Accesory Glands of Male Reproductive Tract*, Ann Arbor Science, Ann Arbor, MI, Vol. 6, pp. 1–28
46. Cunha, G. R., Alarid, E. T., Turner, T., Donjacour, A. A., Boutin, E. L., and Foster, B. A. (1992) *J. Androl.* **13,** 465–475
47. Narla, G., Friedman, S. L., and Martignetti, J. A. (2003) *Am. J. Pathol.* **162,** 1047–1052